Review article

Dario Ballarini and Simone De Liberato*

Polaritonics: from microcavities to sub-wavelength confinement

https://doi.org/10.1515/nanoph-2018-0188
Received November 5, 2018; revised January 8, 2019; accepted January 10, 2019

Abstract: Following the initial success of cavity quantum electrodynamics in atomic systems, strong coupling between light and matter excitations is now achieved in several solid-state set-ups. In those systems, the possibility to engineer quantum emitters and resonators with very different characteristics has allowed access to novel nonlinear and non-perturbative phenomena of both fundamental and applied interest. In this article, we will review some advances in the field of solid-state cavity quantum electrodynamics, focussing on the scaling of the relevant figures of merit in the transition from microcavities to sub-wavelength confinement.

Keywords: cavity quantum electrodynamics; polaritonics; ultrastrong coupling.

1 Introduction

In an idealised cavity quantum electrodynamics (CQED) set-up, in which a collection of dipoles interact with the discrete resonant mode of a photonic cavity, the relevant dimensionless parameter quantifying the intensity of the light–matter interaction is the normalised coupling η [1]. If η, which is the vacuum Rabi frequency Ω divided by the bare transition frequency ω_x, becomes larger than the inverse of the quality factors of the light and matter resonances, the system enters the strong coupling regime. In such a regime, its physics can be correctly described only in terms of the light–matter hybrid eigenmodes of the coupled system, often named polaritons [2]. Higher order effects will become observable when η becomes non-negligible, a regime usually referred to as the ultrastrong, or non-perturbative, regime [1, 3]. Note that the two conditions are a priori independent and, thus, notwithstanding its name, the set of systems exhibiting ultrastrong coupling is not a subset of the strong coupled ones [4]. It is worthwhile to point out that once into the non-perturbative regime, the parameter η defined in Eq. (1) loses some of its relevance, as the approximations to consider a single electronic transition [5–7] or a single resonant cavity mode [8–10] fail.

The intensity of the normalised coupling between an electronic dipolar-active transition and a resonant electromagnetic mode can be calculated to be of the order [11]

$$\eta = \frac{\Omega}{\omega_x} = \mathcal{O}\left(\sqrt{\alpha^3 \frac{N V_\lambda}{V}}\right), \tag{1}$$

where $\alpha \simeq 1/137$ is the fine structure constant, N is the number of effective dipoles coherently coupled to the photonic mode, V is its effective mode volume at the location of the dipoles, and V_λ is the diffraction-limited volume. For Haroche's Rydberg atoms in a superconducting microwave cavity, $\eta < 10^{-6}$: a single atom interacts very weakly with the electromagnetic field. Lowest order perturbation theory is then fully justified, and the achievement of strong coupling is only due to the outstanding lifetimes of the photonic and atomic transitions, with quality factors $Q > 10^8$ [12].

From Eq. (1) we see that, for a given electronic transition (i.e. fixed V_λ), larger couplings can be achieved only by increasing the density $\frac{N}{V}$, which physically measures the overlap between light and matter fields. At a fixed density, instead, η can be increased going towards longer wavelengths, and thus larger V_λ. Apart from determining the intensity of the normalised coupling, photonic mode volume and dipole density play other important roles in determining the physics of the system, creating trade-offs between different figures of merit. Sub-wavelength confinement, which allows achieving $V \ll V_\lambda$, leads to unavoidable losses and thus lowers the quality factor Q [13]. The number of involved dipoles can, instead, change the nature of the system's response, which in the limit $N \to \infty$

*Corresponding author: Simone De Liberato, School of Physics and Astronomy, University of Southampton, Southampton SO17 1BJ, UK, e-mail: S.De-Liberato@soton.ac.uk.
https://orcid.org/0000-0002-4851-2633
Dario Ballarini: CNR NANOTEC-Institute of Nanotechnology, Via Monteroni, 73100 Lecce, Italy

is well described by a bosonised Dicke model [14], while nonlinearities appear as it approaches $N=1$ [15, 16], where it is described by a quantum Rabi model [17].

Using those simple figures of merit as a guide, in this article we will review different combinations of resonator technologies and CQED set-ups used in the literature to achieve strong and ultrastrong coupling. We do not aim at providing a comprehensive review of the developing field of polaritonics, but try to highlight the trade-offs between different design strategies. We will, in particular, highlight the impact of the transition between diffraction-limited cavities and plasmonic sub-wavelength resonators. Given their relevance for plasmonics, we will focus mainly on Wannier and Frankel excitons covering near-infrared and shorter wavelengths. Only in the last part of the article will we briefly consider longer wavelength CQED systems, in which sub-wavelength confinement can be provided either by plasmonic waveguides or by analogous phonon-based resonators. Given the very different physics involved, in this article we will focus on semiconductor-based systems, neglecting both superconducting [18] and magnetic systems [19].

The rest of this article is articulated as follows. In Sections 2 and 3 we will discuss in some further detail the link between sub-wavelength confinement and losses and the novel physics that can be observed in the few-dipoles-strong coupling limit. In Section 4 we briefly describe various excitonic resonances commonly used in CQED and in Section 5 the different kinds of resonators coupled with them. In Section 6 we will pass to review some solid-state CQED platforms working at longer wavelength, where plasmonic resonators effectively behave as waveguides and phonon-based resonators present an interesting dielectric alternative to metallic ones. Finally, in Section 7 we will briefly analyse the different data gathered in the rest of the review and comment on their relevance for the future development of polaritonic science and technology.

2 Sub-wavelength confinement and losses

The most important drawback of the use of plasmonic resonators in CQED is certainly their extremely small quality factor. Losses are seemingly unavoidable because the confinement of the electromagnetic field below the diffraction-limited volume is made possible by storing energy in the kinetic part of a dissipative free-electron gas [13, 20]. The frequency dependance of the interplay between confinement and losses can be understood by using the analytically solvable case of a metallic half-space. Maxwell boundary conditions ensure that a surface-bound solution has to satisfy the relation

$$\varepsilon(\omega)\kappa_{\text{vac}} = -\kappa_{\text{met}}, \tag{2}$$

where κ_{vac} and κ_{met} are the inverse extinction lengths on the vacuum and metallic side, respectively, and $\varepsilon(\omega)$ is the metal dielectric function. As the absolute value of the dielectric function of the Drude model increases at smaller frequencies, with a zero-crossing at the plasma frequency ω_P, Eq. (2) then implies that the electromagnetic field in the lossy metal increases with frequency.

It has been recently shown by Khurgin that this result can be elegantly obtained purely from energy conservation arguments [20]. In particular, the fraction of the total energy that ends up being stored in kinetic form, and thus subject to collisional losses, can be written in terms of the plasma frequency as

$$P_k \simeq \frac{1}{1+2\frac{a^2}{\lambda^2}\frac{\omega_P^2}{\omega^2}}, \tag{3}$$

where the ratio between the confinement length a and the wavelength in the material λ is related to the normalised mode volume $\frac{V}{V_\lambda}$. Consistently with the previous argument, P_k varies from 0 (and thus no collisional losses) for $\omega \ll \omega_P$ to 1 close the plasma frequency.

For metals, ω_P is in the UV, and at mid-infrared and longer wavelengths there is thus very little *plasmon* left, and the resonators are better described as simple metallic waveguides. As we will briefly discuss in Section 6, at those wavelengths a more apt comparison is thus with non-metallic materials characterised by lower values of the plasma frequency.

3 From the Dicke to the Rabi model

In the dilute excitation regime, that is, when the number of dipoles coupled to light is much larger than the number of excitations, the optical response of a collection of dipoles can be described by a bosonic field. Although this could seem a truism in the linear regime, such a correspondence extends to the nonlinear regime, allowing the achievement of stimulated scattering and condensation of hybrid light–matter excitations [2, 21, 22], and more generally treating matter excitations, and a fortiori polaritons, as fully bosonic particles [23–25]. Saturation-induced effects are in those cases limited to highly excited regimes [26, 27] or to very large values of η [16, 28].

At the opposite end of the spectrum, a single dipole, described by the quantum Rabi model [17], provides the perfect nonlinear system, presenting saturation at the single-photon level [29, 30]. Reducing the number of dipoles involved in the formation of a polariton is not only a way to influence its optical spectrum though [15]. In the last decade, various workers have investigated the impact of strong coupling on chemistry and material science [31–35], noticing how certain degrees of freedom of the molecules coupled to the photonic field were affected by the single-molecule coupling strength [36–39].

Moving towards fewer dipoles has thus been an important drive in the development of novel solid-state CQED systems, and probably the one most affected by concomitant advances in plasmonics, which only recently allowed achieving the milestone of single-molecule strong coupling [40]. Note that reducing the number of molecules is not the only way to transition between the Dicke and the Rabi models, which can also be effectively simulated by more complex set-ups [41, 42].

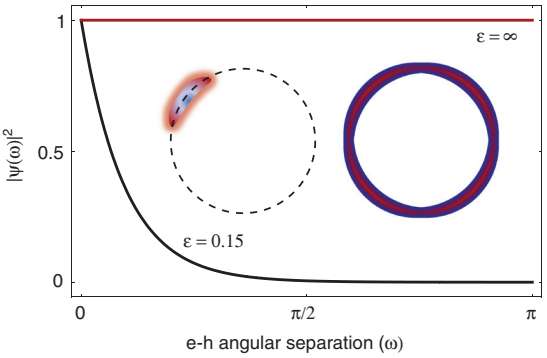

Figure 1: Wavefunction of 3D excitons calculated in spherical coordinates on the surface of a 4D hypersphere (glome) [45]. In the plot, ω is the angular separation between the electron and the hole, with $\omega \approx 0$ for Frenkel excitons and, on the opposite limit, delocalised over the whole space for $\varepsilon = \infty$. The radius of the glome is normalised to 1 for simplicity in both cases and it is related (inversely proportional) to the dielectric constant of the material and the reduced mass of the exciton. In the inset, pictorial representations of the 2D cross-sections of the Frenkel and Wannier–Mott wavefunctions on the glome are shown.

4 Excitons

There are two fundamentally different descriptions of excitons, representing limiting cases of semiconductors with localised or delocalised polarisability: Frenkel and Wannier–Mott [43, 44]. Frenkel excitons exist in materials with low dielectric constant (standard with organic compounds) and are localised on one (or a few) molecules. Wannier–Mott excitons are typical of semiconductors with larger dielectric constant such as III–V and II–VI crystals and are delocalised over hundreds of atomic sites. A visually clear representation of the localised–delocalised transition between the two types of excitons, shown in Figure 1, can be obtained by mapping the 3D exciton wavefunction in the bulk material $\Psi(x, y, z)$ on the surface of a 4D sphere described by three hyperangles, $\Psi(\theta, \phi, \chi)$ [45].

The dimensionality of the system plays a crucial role on the optical properties of excitons, and strictly 2D structures (sub-nanometre thicknesses) such as van der Waals layered materials can combine the best properties of Frenkel and Wannier–Mott excitons. In Table 1, the relevant parameters for excitons in different materials are reported.

In order to be able to compare the number of coupled dipoles in different CQED material systems, it is practical to introduce the concept of oscillator strength.

The oscillator strength f of a transition from the initial state g to a state x can be defined quite generally by a dimensionless quantity in terms of the transition dipole moment $\langle x | \hat{\varepsilon} \cdot \hat{r} | g \rangle$, with $\hat{\varepsilon}$ the polarisation vector of light and r_i the electron position, as

$$f_{\hat{\varepsilon},x} = \frac{2m_e\omega}{\hbar} \left| \left\langle x \middle| \hat{\varepsilon} \cdot \sum_i r_i \middle| g \right\rangle \right|^2 \tag{4}$$

with m_e the electron mass and $\hbar\omega$ the energy difference between the final and the initial state [46]. Physically, the oscillator strength of a transition is the ratio between the absorption rate of that transition and the absorption rate of a single-electron oscillator with the same oscillation frequency ω, thus providing an effective dipole number for many-body excitations.

For fully delocalised excitons, the dimensionless oscillator strength is proportional to the crystal volume, because the centre-of-mass wavefunction (Figure 1) extends over the whole crystal. However, in real systems, the sample size must be replaced by the exciton coherence length L_c, which describes how far the centre of mass of the exciton can move without losing coherence. Delocalised excitons in GaAs quantum well (QW) show coherence lengths of ≈200 nm, while organic excitons are, in the best case of J-aggregates, coherent over few nanometres [47, 48]. The exciton-polariton Rabi frequency is proportional to the exciton oscillator strength, to the total number of dipoles coupled to light, and to the spatial overlap between the material and light field. It follows that a simple reduction of the electromagnetic mode volume in Eq. (1) does not automatically increase the Rabi splitting unless the number N of dipoles is kept constant. The

Table 1: Excitonic properties in inorganic, organic, and hybrid semiconductors.

	GaAs QW	GaN QW	Organic (Lumogen)	Organic (TDAF)	WS2 (TMD)	2D Perovskites
Bohr radius (nm)	12.5	3.5	1	1	1.7	4.5
Binding energy (meV)	5–20	40	830	1000	700	370
Oscill. strength	3×10^{4} μm^{-2}	3×10^{5} μm^{-2}	3×10^{7} μm^{-3}	7×10^{8} μm^{-3}	9×10^{5} μm^{-2}	5×10^{5} μm^{-2}
Hom. FWHM (meV)	0.03	0.3	6	3	3	33
Interactions (μeV μm^{2})	1–10	0.5	10^{-2}	10^{-4}	6×10^{-2}	1
Exciton resonance (eV)	1.5	3.5	2	3.5	2	2.4
Background n_b	3.5	2.7	1.6	2	3.9	1.8

For GaAs and GaN QWs, thicknesses of 7 and 2.7 nm and barriers of AlGaAs and AlGaN are considered, respectively. Organic molecules in the table are small dyes, a perylene derivative (Lumogen Red F305) and 2,7-bis[9,9-di(4-methylphenyl)-fluoren-2-yl]-9,9-di(4-methylphenyl)fluorene (TDAF). The monolayer of WS_2 is measured without the cladding layer. The 2D perovskite is a large single crystal of phenethylammonium lead iodide $(C_6H_5(CH_2)_2NH_3)_2PbI_4$ (PEAI) self-assembled by an anti-solvent-vapor-assisted crystallisation method and subsequent mechanically exfoliated to produce thin flakes of 100 nm. The oscillator strength of layered perovskites is normalised to the number of inorganic layers, in analogy to GaAs QWs. For a single monolayer of tungstene disulfide (WS_2), the background refractive index is given as obtained from spectroscopic ellipsometry for completeness, but its role in the exciton formation is negligible since most of the field lies outside the monolayer.

meaningful quantity is therefore the oscillator strength per unit volume $\tilde{f}$, that is, the oscillator strength of a single dipole times the number of excitons that can be filled in the unit volume.

For practical purposes, the oscillator strength per unit volume, $\tilde{f}$, is obtained from the absorption coefficient $\alpha(\omega)$ integrated over the excitonic peak as [46, 49, 50]

$$\int\alpha(\omega)\mathrm{d}\omega=\frac{\pi e^2}{2\varepsilon_0 n_b m_e c}\tilde{f}, \tag{5}$$

where n_b is the background refraction index, ε_0 is the vacuum permittitivity, and c is the speed of light. In a QW, the oscillator strength is, instead, proportional to the considered surface, and it is thus expressed per unit area per QW. Typical values for excitons in GaAs QWs with thickness of 7 nm are of the order of $\tilde{f}\approx10^{4}$ μm^{-2}. In order to increase the coupling strength, multiple QWs can be embedded in the same planar resonator, leading to a total scaling

$$\eta\propto\sqrt{\frac{N\tilde{f}}{L}}, \tag{6}$$

where N is the number of QWs and L is the effective cavity thickness.

On the opposite end of the spectrum, in organic compounds, an exciton is often localised on a single molecule (Figure 1) with $f\approx0.5$–1.5. The oscillator strength is therefore measured per unit volume according to Eq. (5), with $\tilde{f}=\frac{N}{V}\times f$ and $\frac{N}{V}$ the molecular density. As shown in Table 1, in the same volume of a microcavity (≈μm^3) the equivalent number of oscillators is about three orders of magnitude larger for Frenkel excitons in organic molecules than for Wannier–Mott excitons in GaAs QWs. This allows the Rabi splitting in organic microcavities to reach hundreds of meV and, in some cases, to enter into the ultrastrong coupling regime in the visible range with $\eta\approx0.3$ [51, 52].

Importantly, the photon–exciton interaction scales as an inverse power of the Bohr radius a_b, while the Coulomb interaction between excitons roughly scale as $E_b a_b^2$, where E_b is the exciton binding energy [53–57]. As such, the large a_b of excitons in GaAs QWs makes it challenging to achieve ultrastrong coupling with these materials [58], but at the same time they are particularly suited for *dressing* the photons with nonlinearities three orders of magnitude higher than in standard optical crystals [59]. In the past decade, these have allowed the demonstration of a large number of active optical functionalities, from spin switches to all-optical logic gates, and from polariton multi-stability to polariton simulators of many-body Hamiltonians [60–65]. This has been possible thanks to the high degree of control on the material purity and the advances in the deposition and processing techniques that have allowed GaAs/GaAlAs- and InGaAs/GaAs-based structures to lead the field. The exciton binding energy is, however, relatively low, of a few meV, limiting their operation to cryogenic temperatures, but also allowing the observation of other interesting interaction-induced phenomena [58, 66]. The strong coupling regime with higher band-gap semiconductors such as GaN and ZnO has been largely studied at room temperature [67–69]. Despite the fact that the optical quality is in general substantially lower than for GaAs-based structures, these materials hold a strong potential for technological

applications and have shown room-temperature polariton lasing, under both optical and electrical injection in the case of GaN [70–72]. The huge binding energy of Frenkel excitons makes organic molecules a promising alternative for polaritons at room temperature [22, 73–75], and their smaller Bohr radius allows them to reach the ultrastrong light–matter coupling regime [51, 52]. Still, the smaller a_b means as well much smaller exciton–exciton interactions, challenging the implementation of nonlinear optical effects in room-temperature polariton systems. However, new perspectives are opened by the peculiarities of strong coupling in organic materials, where the large energy splitting can alter the relaxation dynamics and optical efficiencies, but also can act as all-optical switching of the reaction dynamics [76–78]. Moreover, the synthetic versatility of organic molecules facilitates their integration in optical resonators with smaller modal volumes, such as plasmonic cavities, allowing increase of the normalised coupling η up to the ultrastrong regime with only a bunch of molecules. Relevant data for various excitonic resonances can be found in Table 1.

The best properties of Frenkel and Wannier–Mott excitons are mixed when the exciton is extremely confined on a lower dimensionality, such as in monolayers of transition-metal dichalcogenides (TMDs). In these 2D semiconductors, the electronic screening is reduced by dimensionality, and typical binding energies are hundreds of meV, allowing strong coupling to be observed at room temperature. In analogy to the strategy adopted with epitaxial QWs, stacking N monolayers increases the coupling by a factor $\sqrt{N}$ [79]. Interestingly, layered perovskites form naturally ordered structures of 2D inorganic layers separated by chains of organic molecules. These hybrid materials are excellent semiconductors in the visible range, and strong coupling with single crystals of 2D perovskites has shown comparable characteristics to GaAs QWs but working at room temperature [80–82]. The nonlinearities associated with these *flat* excitons are similar to those of Wannier–Mott excitons in GaAs QWs, including the spin-dependent strength of the interaction between excitons, opening the door to all-optical spin manipulation at room temperature [83–85].

5 Resonator technologies

In Figure 2, the strong coupling regime with organic and inorganic excitons is shown for different resonator technologies, going from dielectric cavities to surface evanescent modes and plasmonic cavities with ultrasmall mode volumes. The parabolic dispersion of a photon in a cavity is partially retained by the lower polariton branch (LPB), as shown in Figure 2D. The effective mass of polaritons close to the bottom of the LPB is only a tiny fraction of the exciton's mass, enabling stimulated scattering to prevail over losses even at room temperature. Polariton condensation requires, however, long lifetimes to reach the critical density at the bottom of the LPB. The microcavities with the highest optical quality are obtained by epitaxial deposition of two dielectric mirrors (dielectric Bragg reflectors, DBRs) composed of alternating layers of GaAs and AlGaAs, and polariton condensation was initially demonstrated in a GaAs-based microcavity at 4 K with CdTe QWs [89, 90]. After the observation of polariton condensation, out-of-equilibrium quantum fluids have been largely explored in these solid-state systems [2]. Among other results, superfluidity, Josephson oscillations, quantised vorticity, and optical spin-Hall effect are only some examples of the rich physics that can be investigated with microcavity polaritons [91–98]. Recently, GaAs microcavities with extremely long polariton lifetimes ≈200 ps have allowed approaching the physics of equilibrium quantum fluids, opening new possibilities for the manipulation of large polariton condensates [99–103]. Moreover, the fine control over the lithographic patterning of these structures has prompted the realisation of topological structures, with promising results recently reported [104–106].

The DBR technology, while ensuring high quality factors and long polariton lifetimes, is limited to mode volumes comparable to the cubic wavelength of light in the material. In these structures, the normalised coupling with embedded GaAs QW excitons can reach values $\eta \simeq 0.1$–1%, allowing the strong coupling regime to be measured only with relatively high quality factors $Q > 10^3$. Strong coupling with a single quantum dot (QD) has been observed in a high-Q micropillar and photonic crystal cavities at low temperatures [107–112]. More recently, attempts to use polariton nonlinearities to realise squeezed light or polariton blockade have been reported [113–118]. It has been shown also that single and entangled photons can be injected from outside into the polariton mode and quantum correlations deployed by the coupling with a condensate [119]. On the opposite side, with many millions of dipoles coupled to the electromagnetic field, DBRs with lower quality factors ($Q \approx 600$) already show polariton condensation at room temperature [22, 120, 121]. Note that, despite that polariton nonlinearities associated with molecular excitons have been measured to be two to three orders of magnitude weaker than for inorganic excitons, the large density of oscillators has enabled the observation of collective effects such as superfluid flow across a defect

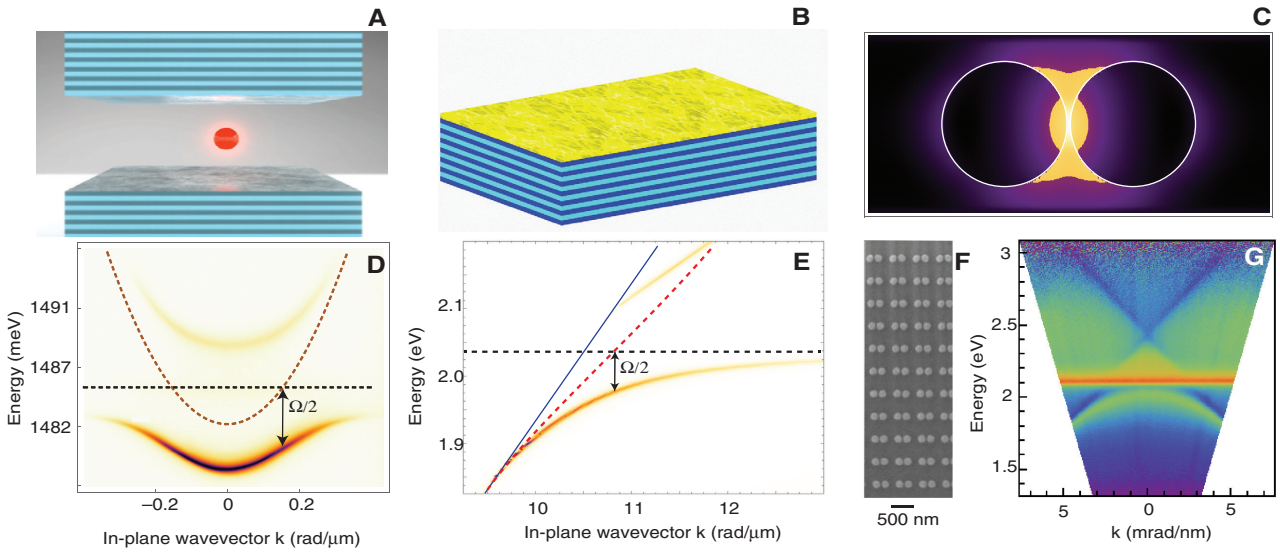

Figure 2: Photonic structures showing strong coupling with a matter resonance in the visible range.
(A) Cavity made of two DBR mirrors with the exciton dipole represented by the red sphere. (B) Bloch surface wave (BSW) sustained on the top of a single DBR, with the thin active layer deposited at the maximum enhancement of the electromagnetic field. (C) Spatial distribution of the electromagnetic field (numerically simulated by FDTD) at resonance with a gap-plasmon, with the maximum enhancement localised within the two metallic nanoparticles. (D) Dispersion of the microcavity polariton associated with the structure in (A): the parabolic dispersion of a photon in a cavity (red dashed line) and the flat dispersion of the exciton (black dashed line) in this angular range show a clear anti-crossing with vacuum Rabi energy $\hbar\Omega = 4$ meV and exciton-cavity detuning $\delta = -3$ meV [86]. (E) Dispersion of organic BSW polaritons. The light line is defined by the interface between the heterostructure and air (blue line). The Rabi energy anti-crossing between the the BSW (red dashed line) and the exciton (black dashed line) is $\Omega = \hbar 50$ meV [87]. (F) SEM image of an array of plasmonic nanoparticle dimers as in (C), where hybridisation can occur between the localised plasmons, the surface modes associated with the lattice, and the organic molecular exciton of the deposited material. (G) Dispersion of the structure in (F), with an organic molecular layer deposited on top of the array of coupled nanoparticles. The anti-crossing is small compared to the line width but still visible [88]. Additional details on the parameter structures can be found in Refs [86–88].

[122]. An alternative to full microcavities are waveguide modes and evanescent modes at the interface between a metal and a dielectric or at the interface between a DBR and air [123–127]. These structures are particularly suited for in-plane propagation and are useful when the realisation of the top DBR in standard cavities may damage the active material. Strong coupling with a Bloch surface wave (BSW) has allowed the measurement of nonlinearities with organic molecules and TMD monolayers in propagating polariton fluids [87, 128]. Strong coupling involving both GaAs QWs and TMD monolayers has also been demonstrated in hybrid structures [129, 130]. When strong coupling involves a surface plasmon (SP), the mode volume is reduced with respect to optical microcavities and BSW, reaching sub-wavelength values at the price of much smaller quality factors [131–136]. This trends is evident in Figure 3, where the effective volumes are shown as a function of the quality factor for several of the works discussed in this section and reported in Table 2.

To allow comparison between different resonator technologies, the confinement for planar optical cavities is considered only in the direction perpendicular to the

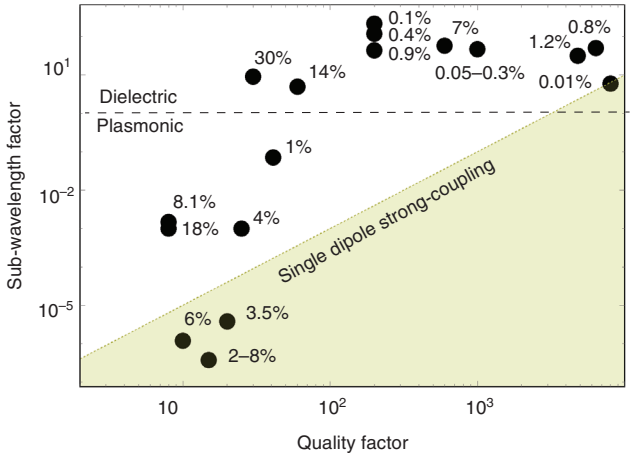

Figure 3: Sub-wavelength factor $\frac{V}{V_\lambda}$ versus the quality factor of the photonic resonators for the works in Table 2.The normalised coupling η is shown as well for each point. The horizontal line indicates the minimum sub-wavelength factor achievable with dielectric structures ($\approx$1). The dashed line represents the scaling of V in order to keep the condition of strong coupling with a single dipole ($N = 1$) for a given $f \approx 1$. Note that, at the top-right corner, the small η of InGaAs QD is compared with the almost ultrastrong coupling regime of single molecule at the left-bottom corner.

Table 2: Estimated figures of merit for representative exciton–polariton systems, from dielectric DBR microcavities to plasmonic arrays and localised plasmonic cavities.

Resonator	Exciton	Material	V/V_λ	N	Q	$\hbar\omega_x$ (meV)	η (%)	Room temp.	Ref.
NPoM	OM	Methylene blue	4×10^{-7}	1	15	1.9	2	Y	[40]
NPoM	OM	Methylene blue	4×10^{-7}	10	15	1.9	8	Y	[40]
LP	OM	Cyanine dye	10^{-3}	6×10^{3}	8	1.55	18	Y	[137]
LP	OM	HITC molecules	10^{-3}	188	8	1.67	8.1	Y	[138]
SM	OM	Squaraine dye	9	1.4×10^{8}	30	1.85	30	Y	[51]
SM	OM	TDAF	5	1.9×10^{7}	60	3.5	14	Y	[52]
DBR	OM	TDAF	30	3.2×10^{7}	600	3.5	7	Y	[22]
MD	QD	InGaAs	6	100	8000	1.67	0.01	N	[107]
LP	QD	ZnS	3.8×10^{-6}	3	20	1.55	3.5	Y	[139]
GP	QD	CdS	1.2×10^{-6}	8	10	1.9	6	Y	[140]
DBR	28 QW	GaAs	47	7.8×10^{5}	1000	1.61	0.3	N	[58]
DBR	QW	GaAs	47	2.8×10^{4}	1000	1.61	0.05	N	[58]
DBR	Bulk	GaAs	218	8.4×10^{3}	200	1.5	0.1	N	[141]
DBR	Bulk	GaN	119	9×10^{3}	200	3.5	0.4	Y	[141]
DBR	Bulk	ZnO	44	2×10^{4}	200	3.3	0.9	Y	[141]
OC	TMD	$MoSe_2$	51	8.4×10^{5}	6375	1.66	0.8	Y	[142]
NPoM	TMD	WSe_2	10^{-3}	182	25	1.63	4	Y	[79]
LP	TMD	MoS_2	0.07	232	41	1.97	1	Y	[143]
DBR	TMD	MoS_2	31	7.8×10^{4}	4800	1.87	1.2	Y	[144]

MD, MicroDisk; DBR, DBR microcavities; OC, open DBR microcavity; SM, microcavity with semitransparent silver mirrors; LS, localised plasmon array; GP, gap-plasmon; NPoM, nanoparticle on mirror; OM, organic molecules, TMD, monolayer of transition-metal dichalcogenide; QW, quantum well; QD, quantum dot.

cavity plane, while taking a conventional surface area given by $S=\pi\lambda_0^2$ for the resonant wavelength in air λ_0, as the minimal diffraction-limited surface of the pump. Note that, in the case of DBR structures, the effective mode volume, which has to include the penetration length in the dielectric mirrors, is usually not explicitly reported in the literature, and it has thus to be estimated from available data. The number of dipoles is meant as the equivalent number of electron oscillators as obtained directly from the measured oscillator strengths.

Even with sub-wavelength volumes and strong oscillator strengths, the limit for achieving strong coupling with a single dipole at room temperature is stringent. At room temperature, thermal fluctuations reduce the maximum quality factor, meaning that strong coupling can be achieved only by reducing the mode volume. As $\eta\propto\frac{1}{\sqrt{V}}$ and in the strong coupling regime $\eta>\frac{1}{Q}$, in Figure 3 the scaling of the maximum volume for strong coupling with a single molecule is drawn as $V\propto Q^2$. The extreme localisation of the electromagnetic field is achieved with plasmonic cavities. Metallic nanoparticles sustain highly localised plasmonic modes with mode volumes of few hundreds of nanometre cubes, leading to extremely small sub-wavelength confinement. Ultrastrong coupling with localised plasmons and organic excitons has been theoretically investigated [145] and recently demonstrated with normalised coupling $\eta\simeq0.18$ [137].

The interaction between different localised plasmons can be handled following different strategies. In arrays of metallic nanoparticles, hybridisation between the diffracted modes of the array and localised plasmons allow the reduction of the losses inherent in the metallic absorption while keeping a relatively small mode volume, allowing strong coupling to be obtained with organic molecules and TMD monolayers [88, 143, 146, 147]. Recently, interaction and coherence of polariton condensates have been shown in such structures at room temperature [148]. To further reduce the field volume, two metallic nanoparticles (or a nanoparticle on a flat metallic mirror) can be brought close enough to allow direct hybridisation of the localised plasmon modes, boosting the electric field in the inter-particle gap by several orders of magnitude. Gap-plasmon cavities have the lowest mode volume, and strong coupling with a single molecule has been recently demonstrated at room temperature using such plasmonic resonators [40]. This is possible thanks to the relatively high normalised coupling, arising from the highly confined electromagnetic field and despite the low dipole density (see Figure 3). This result opens broad fundamental and technological perspectives spanning from quantum plasmonics to

photochemistry and suggests that the ultrastrong coupling regime could be achieved in such resonators with a relatively small number of dipoles.

6 Long-wavelength polaritonics

At longer wavelengths, the distinction between plasmonic and standard resonators loses some of its relevance, because, as visible from Eq. (3), only a limited portion of the field energy is stored in kinetic form. Nevertheless, in the field of mid-infrared and terahertz polaritons, the use of sub-wavelength resonators, which still have limited quality factors when compared with DBR, has led to important results which we will briefly examine for the two most relevant cases of intersubband and Landau polaritons. We will finally mention recent advances in phonon-polariton resonators, which, due to their longer lifetimes and lower plasma frequencies, provide an interesting analogue to plasmonic resonators at longer wavelengths.

6.1 Intersubband polaritons

Intersubband polaritons are hybrid quasi-particles resulting from the strongly coupled transition between multiple conduction subbands in doped QWs. The schematic of a simple two-subband intersubband transition is sketched in Figure 4A. Easily tunable though the terahertz and mid-infrared portions of the spectrum by engineering the QW design, those excitations are the object of intense research interest due to their potential as a novel platform for mid-infrared and terahertz nanophotonics [149–155]. Moreover, the vacuum Rabi frequency in those systems is proportional to the square root of the electron density, allowing for a conceptually and technologically straightforward way to access the ultrastrong coupling regime [156] and to modify the coupling on-site [157].

Because of their TM selection rule and their comparatively long wavelength, DBRs are not viable alternatives in those systems, which led to the exploration of a number of different designs. Intersubband polaritons were observed for the first time in 2003 [158] using doped GaAs QWs and confining the electromagnetic field exploiting total internal reflection. Using, instead, a top metallic mirror, this was also first system in which the ultrastrong coupling regime was observed, with $\eta \simeq 0.11$ [159].

Sub-wavelength cavities are often employed in intersubband polaritons, using either sub-wavelength metallic patches over a metal ground [154, 160], 3D nanoantennas [161], or LC meta-material resonators [162, 163]. In Table 3 we provide the parameters for some representative intersubband polariton experiments using different resonator technologies.

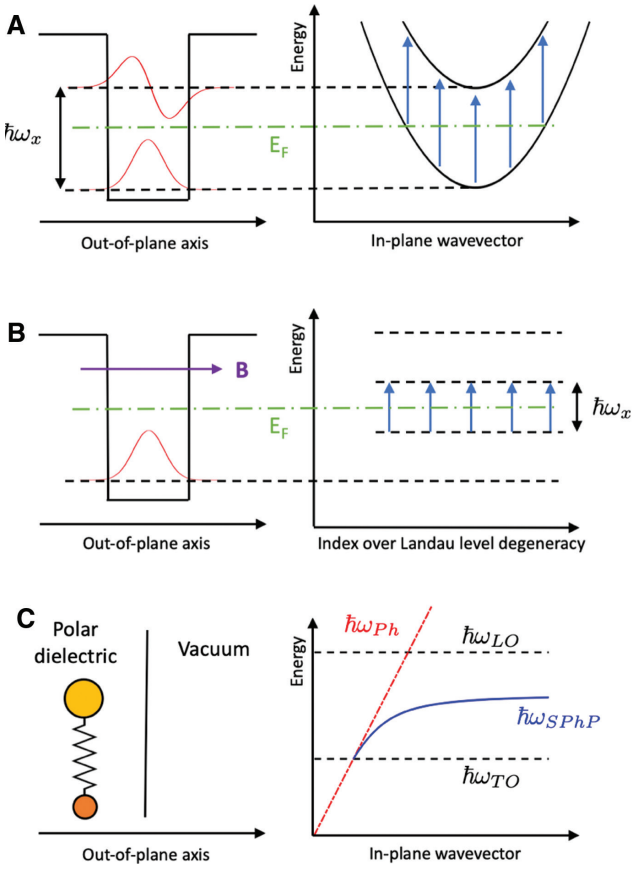

Figure 4: Sketch of the three different long-wavelength polaritonic platforms discussed in the main text.
(A) Intersubband transition between two conduction subbands in a doped quantum well. (B) Transition between different Landau levels in a 2D electron gas under applied magnetic field. (C) Surface phonon–polariton resonance $\hbar\omega_{SPhP}$ at the interface between a polar dielectric and vacuum. In the figure, E_F is the Fermi energy, **B** is the applied magnetic field, and $\hbar\omega_{Ph}$, $\hbar\omega_{LO}$, and $\hbar\omega_{TO}$ are, respectively, the energies of the photon and of the longitudinal and transverse optical phonons.

Table 3: Figures of merit for representative intersubband polariton samples using different resonators.

Resonator	V/V_λ	N	Q	$\hbar\omega_x$ (meV)	η (%)	Ref.
Planar	1	10^8	15	152	11	[159]
Nanopatch	10^{-4}	10^7	12	12	24	[160]
LC Metamaterial	10^{-5}	2400	10	125	8	[162]

6.2 Landau polaritons

Landau polaritons exploit as matter component the transitions between Landau levels in charged gases

Table 4: Figures of merit for representative Landau polariton resonators.

Resonator	V/V_λ	N	Q	$\hbar\omega_x$ (meV)	η (%)	Ref.
DBR	1	10^8	183	1.6	9	[169]
LC Metamaterial	2×10^{-6}	2×10^7	3	2.0	143	[168]
LC Metamaterial	6×10^{-10}	90	8	1.2	36	[171]

under applied magnetic fields, as sketched in Figure 4B [164]. On the photonic side, various kinds of both diffraction-limited and sub-wavelength resonators have been used, including stripline resonators [165], split-ring resonator metamaterials [166–168], and DBR resonators [169, 170].

According to the different resonators employed, Landau polaritons have achieved the record normalised coupling between present CQED systems ($\eta \simeq 1.43$ [168]) and also remarkable results in terms of the number of electrons coupled to the resonator ($N \simeq 90$ [171]) and quality factors at long wavelengths ($Q \simeq 183$ [169]). Parameters for those three samples are collected in Table 4.

6.3 Phonon-polaritons

Phonon-polaritons are essentially mid-infrared analogues of plasmons, which exploit the movement of ions in the crystal lattice to confine the electromagnetic field instead of the movement of free charges in a metal. Such phonon-polaritons exist only at longer wavelengths, in the Reststrahlen band of polar dielectics, and are characterised by much longer lifetimes, not being subject to Ohmic losses. Although those excitations lead to smaller field enhancement because a part of the electric energy ends up as potential ionic deformation energy [20], they can still provide comparable sub-wavelength confinement and tunability [172–177]. Moreover, thanks to phonon anharmonicity, they can provide polaritons with large nonlinear interactions [178, 179].

A relatively recent addition to the catalogue of CQED technologies, surface phonon-polaritons, whose dispersion is shown in Figure 4C, have been strongly coupled to a number of other excitations, including plasmonic nanorods [180], graphene plasmons [181], localised phonon-polariton modes [182], and ENZ (epsilon-near-zero) modes [183]. Localised phonon-polaritons have also been coupled to intersubband transition in a quantum cascade laser architecture [184, 185] although without achieving strong coupling.

7 Conclusions

Data reported in Tables 2–4 are represented in Figures 3 and 5 along multiple dimensions. Spanning multiple orders of magnitudes along dipole number, confinement factor, wavelength, and normalised coupling strength, polaritonic platforms have pushed to the extreme different boundaries of light–matter interaction.

Although any simple heuristic is bound to be inaccurate when used to analyse such a heterogeneous set, we can see that expected patterns emerge. In Figure 3, the trade-off between sub-wavelength confinement and losses, described by Eq. (3), is apparent. From the same image we can see that, even though strong coupling with single emitters can be *a priori* achieved with different resonator technologies, only in deeply sub-wavelength plasmonic resonators the coupling strength can be made large enough to be useful for proposed applications in chemistry and modification of electronic properties [36–39]. In Figure 5, the different samples, including mid-infrared ones, are represented as a function of their sub-wavelength factor, dipole number, and normalised coupling. Diagonal lines represent ideal $N \propto \frac{V}{V_\lambda}$ dependencies at

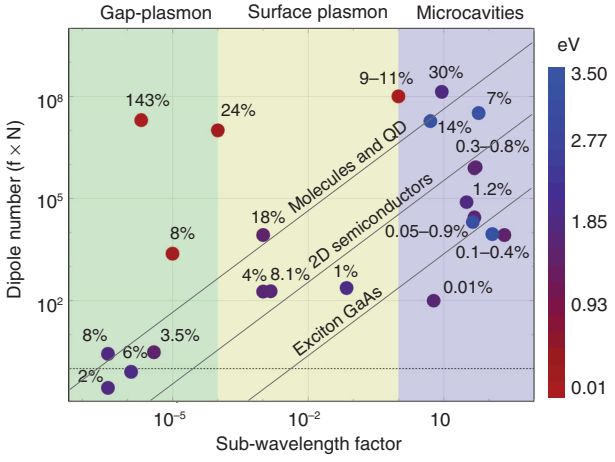

Figure 5: Number of effective dipoles ($N\times f$) vs sub-wavelength confinement factor as reported in Tables 2–4.The normalised coupling η is shown in the label on each point. The vertical shaded regions indicate the sub-wavelength range for dielectric microcavities (purple), plasmonic surface modes (yellow), and extremely localised plasmonic nanoantennas (green). The energy of the electronic resonance is shown for each point by the color code on the right of the figure. The grey lines represent the scaling of volume and dipole number, at a given frequency and constant η. Given that the dipole density is roughly constant for each materials, each line represents increasing light–matter interaction going from the bottom-left corner to the top-right corner. The horizontal line indicates the unitary strength of an ideal single electronic oscillator, $N\times f=1$.

equal η for different representative resonances, from Eq. (1). Even though the ultrastrong coupling regime has been achieved in planar microcavities using organic molecules, it is clear how going towards lower frequencies, thus reducing the denominator of $\eta = \frac{\Omega}{\omega_x}$, allows us to achieve coupling well beyond of what possible at shorter wavelengths.

In this article we have provided a cursory look at recent developments in the field of solid-state CQED, paying particular attention to figures of merit and trade-offs relevant for different optically active transitions in diffraction-limited and sub-wavelength resonators. We discussed the design choices required to access the scientifically and technologically interesting regimes of ultrastrong and single-molecule strong coupling and hopefully provided useful tools for the design of future CQED platforms.

Acknowledgements: SDL is a University Research Fellow of the Royal Society and acknowledges support from the Innovation Fund of the EPSRC Programme EP/M009122/1. DB acknowledges the ERC project ElecOpteR grant number 780757. The authors are grateful to C. Gubbin, D. Gerace, and D. Sanvitto for fruitful discussions, and to F. Riminucci for FTDT calculations.

References

[1] Kockum AF, Miranowicz A, De Liberato S, Savasta S, Nori F. Ultrastrong coupling between light and matter. Nat Rev Phys 2019;1:19–40.
[2] Carusotto I, Ciuti C. Quantum fluids of light. Rev Mod Phys 2013;85:299–366.
[3] Forn-Díaz P, Lamata L, Rico E, Kono J, Solano E. Ultrastrong coupling regimes of light-matter interaction. 2018;arXiv:1804.09275.
[4] De Liberato S. Virtual photons in the ground state of a dissipative system. Nat Commun 2017;8:1465.
[5] De Bernardis D, Jaako T, Rabl P. Daniele De Bernardis, Tuomas Jaako, Peter Rabl. Cavity quantum electrodynamics in the nonperturbative regime. Phys Rev A 2018;97:043820.
[6] De Bernardis D, Pilar P, Jaako T, De Liberato S, Rabl P. Breakdown of gauge invariance in ultrastrong-coupling cavity QED. Phys Rev A 2018;98:053819.
[7] Di Stefano O, Settineri A, Macrì V, Garziano L, Stassi R, Savasta S, Nori F. Resolution of Gauge Ambiguities in Ultrastrong-Coupling Cavity QED. 2018;arXiv:1809.08749.
[8] Sundaresan NM, Liu Y, Sadri D, et al. Beyond strong coupling in a multimode cavity. Phys Rev X 2015;5:021035.
[9] George J, Chervy T, Shalabney A, et al. Multiple rabi splittings under ultrastrong vibrational coupling. Phys Rev Lett 2016;117:153601.
[10] Sánchez Muñoz C, Nori F, De Liberato S. Resolution of superluminal signalling in non-perturbative cavity quantum electrodynamics. Nat Commun 2018;9:1924.
[11] Devoret MH, Girvin S, Schoelkopf R. Circuit-QED: Howstrong can the coupling between a Josephson junction atom and a transmission line resonator be? Ann Phys 2007;16:767–9.
[12] Haroche S, Raimond JM. Exploring the quantum: atoms, cavities, and photons. Oxford: Oxford University Press, 2006.
[13] Khurgin JB. How to deal with the loss in plasmonics and metamaterials. Nat Nanotechnol 2015;10:2 EP.
[14] Kirton P, Roses MM, Keeling J, Dalla Torre EG. Introduction to the Dicke model: from equilibrium to nonequilibrium, and vice versa. 2018:arXiv:1805.09828.
[15] Todorov Y, Sirtori C. Few-electron ultrastrong light-matter coupling in a quantum *LC* circuit yanko todorov and carlo sirtori. Phys Rev X 2014;4:041031.
[16] Cortese E, Garziano L, De Liberato S. Polariton spectrum of the Dicke-Ising model Erika Cortese, Luigi Garziano, and Simone De Liberato. Phys Rev A 2017;96:053861.
[17] Rossatto DZ, Villas-Bôas CJ, Sanz M, Solano E. Cooling by heating in the quantum optics domain. Phys Rev A 2017;96:013849.
[18] Yoshihara F, Fuse T, Ashhab S, Kakuyanagi K, Saito S, Semba K. Superconducting qubit-oscillator circuit beyond the ultrastrong-coupling regime. Nat Phys 2016;13:44 EP.
[19] Zhang X, Zou C-L, Jiang L, Tang HX. Strongly coupled magnons and cavity microwave photons. Phys Rev Lett 2014;113:156401.
[20] Khurgin J. Relative merits of phononics vs. plasmonics: the energy balance approach. Nanophotonics 2017;7:305.
[21] Kéna-Cohen S, Forrest SR. Room-temperature polariton lasing in an organic single-crystal microcavity. Nat Photonics 2010;4:371 EP.
[22] Daskalakis KS, Maier SA, Murray R, Kéna-Cohen S. Nonlinear interactions in an organic polariton condensate. Nat Mater 2014;13:271–8.
[23] De Liberato S Ciuti C. Stimulated scattering and lasing of intersubband cavity polaritons. Phys Rev Lett 2009;102:136403.
[24] Shammah N, Lambert N, Nori F, De Liberato S. Superradiance with local phase-breaking effects. Phys Rev A 2017;96:023863.
[25] Dominici L, Colas D, Donati S, et al. Ultrafast control and rabi oscillations of polaritons. Phys Rev Lett 2014;113:226401.
[26] Deng H, Weihs G, Snoke D, Bloch J, Yamamoto Y. Polariton lasing vs. photon lasing in a semiconductor microcavity. Proc Natl Acad Sci 2003;100:15318–23.
[27] Zanotto S, Degl'Innocenti R, Xu J-H, Sorba L, Tredicucci A, Biasiol G. Ultrafast optical bleaching of intersubband cavity polaritons.Phys Rev B 2012;86:201302.
[28] Di Stefano O, Stassi R, Garziano L, Kockum AF, Savasta S, Nori F. Feynman-diagrams approach to the quantum Rabi model for ultrastrong cavity QED: stimulated emission and reabsorption of virtual particles dressing a physical excitation. New J Phys 2017;19:053010.
[29] Birnbaum KM, Boca A, Miller R, Boozer AD, Northup TE, Kimble HJ. Photon blockade in an optical cavity with one trapped atom. Nature 2005;436:87–90.
[30] Ridolfo A, Leib M, Savasta S, Hartmann MJ. Photon blockade in the ultrastrong coupling regime. Phys Rev Lett 2012;109:193602.
[31] Ebbesen TW. Hybrid light–matter states in a molecular and material science perspective. Acc Chem Res 2016;49:2403–12.
[32] Thomas A, George J, Shalabney A, et al. Ground-state chemical reactivity under vibrational coupling to the vacuum electromagnetic field. Angew Chem Int Ed 2016;55:11462–6.

[33] Galego J, Garcia-Vidal FJ, Feist J. Many-molecule reaction triggered by a single photon in polaritonic chemistry. Phys Rev Lett 2017;119:136001.
[34] Ribeiro RF, Martãnez-martãnez LA, Du M, Campos-Gonzalez-Angulo J, Yuen-Zhou J. Polariton chemistry: controlling molecular dynamics with optical cavities. Chem Sci 2018;9:6325–39.
[35] Feist J, Galego J, Garcia-Vidal FJ. Polaritonic chemistry with organic molecules. ACS Photonics 2018;5:205–16.
[36] Galego J, Garcia-Vidal FJ, Feist J. Cavity-induced modifications of molecular structure in the strong-coupling regime. Phys Rev X 2015;5:041022.
[37] Ćwik JA, Kirton P, De Liberato S, Keeling J. Excitonic spectral features in strongly-coupled organic polaritons. Phys Rev A 2016;93:033840.
[38] Cortese E, Lagoudakis PG, De Liberato S. collective optomechanical effects in cavity quantum electrodynamics. Phys Rev Lett 2017;119:043604.
[39] Martínez-Martínez LA, Ribeiro RF, Campos-González-Angulo J, Yuen-Zhou J. Polariton chemistry: controlling molecular dynamics with optical cavities. Chem Sci 2018;9:6325–39.
[40] Chikkaraddy R, de Nijs B, Benz F, et al. Single-molecule strong coupling at room temperature in plasmonic nanocavities. Nature 2016;535:127–30.
[41] Crespi A, Longhi S, Osellame R. Photonic realization of the quantum rabi model. Phys Rev Lett 2012;108:163601.
[42] De Liberato S, Ciuti C. Quantum phases of a multimode bosonic field coupled to flat electronic bands. Phys Rev Lett 2013;110:133603.
[43] Yu P, Cardona M. Fundamentals of semiconductors. Berlin, Springer, 1996.
[44] Weisbuch C, Vinter B. Quantum semiconductor structures. Boston, Academic Press, 1991.
[45] Loos P-F. Understanding excitons using spherical geometry. Phys Lett A 2012;376:1997.
[46] Andreani LC. Confined electrons and photons. In: Burstein E, Weisbuch C, eds. New York: Plenum, 1995, p. 57.
[47] Deveaud B, Clérot F, Roy N, Satzke K, Sermage B, Katzer DS. Enhanced radiative recombination of free excitons in GaAs quantum wells. Phys Rev Lett 1991;67:2355.
[48] De Boer S, Wiersma DA. Dephasing-induced damping of superradiant emission in J-aggregates. Chem Phys Lett 1990;165:45–53.
[49] Weisbuch C, Benisty H, Houdré R. Overview of fundamentals and applications of electrons, excitons and photons in confined structures. J Lumin 2000;85:271–93.
[50] Hoffmann M, Schmidt K, Fritz T, Hasche T, Agranovich V, Leo K. The lowest energy Frenkel and charge-transfer excitons in quasi-one-dimensional structures: application to MePTCDI and PTCDA crystals. Chem Phys 2000;258:73–96.
[51] Gambino S, Mazzeo M, Genco A, et al. Exploring Light–Matter Interaction Phenomena under Ultrastrong Coupling Regime. ACS Photonics 2014;1:1042–8.
[52] Kéna-Cohen S, Maier SA, Bradley DDC. Ultrastrongly Coupled Exciton–Polaritons in Metal-Clad Organic Semiconductor Microcavities. Adv Opt Mater 2013;1:827–33.
[53] Weisbuch C, Houdré R, Stanley RP. Spontaneous emission and laser oscillation in microcavities. In: Yokoyama H, Ujihara K, eds. USA, CRC Press, 1995, Chapter 4, pp. 109–150.
[54] Chemla D. Quasi-two-dimensional excitations in GaAs/Al_xGa_1-xAs semiconductor multiple quantum well structures Helv Phys Acta 1983;6:607–37.
[55] Ciuti C, Savona V, Piermarocchi C, Quattropani A, Schwendimann P. Role of the exchange of carriers in elastic exciton-exciton scattering in quantum wells. Phys Rev B 1998;58:7926.
[56] Tassone F, Yamamoto Y. Exciton-exciton scattering dynamics in a semiconductor microcavity and stimulated scattering into polaritons. Phys Rev B 1999;59:10830.
[57] Andreani LC, Panzarini G, Gérard J-M. Strong-coupling regime for quantum boxes in pillar microcavities: Theory. Phys Rev B 1999;60:13276.
[58] Brodbeck S, De Liberato S, Amthor M, et al. Experimental verification of the very strong coupling regime in a gaas quantum well microcavity. Phys Rev Lett 2017;119:027401.
[59] Snoke D. Polariton condensation and lasing. Exciton polaritons in microcavities, Springer series in solid state sciences. Berlin, Springer, 2012, Chapter 12.
[60] Amo A, Liew TCH, Adrados C, et al. Exciton-polariton spin switches. Nat Photonics 2010;4:361.
[61] De Giorgi M, Ballarini D, Cancellieri E, et al. Control and ultrafast dynamics of a two-fluid polariton switch. Phys Rev Lett 2012;109:266407.
[62] Ballarini D, De Giorgi M, Cancellieri E, et al. All-optical polariton transistor. Nat Commun 2013;4:1778.
[63] Paraïso TK, Wouters M, Léger Y, Morier-Genoud F, Deveaud-Plédran B. Multistability of a coherent spin ensemble in a semiconductor microcavity. Nat Mater 2010;9:655–60.
[64] Berloff NG, Silva M, Kalinin K, et al. Realizing the classical XY Hamiltonian in polariton simulators. Nat Mater 2017;16:1120–6.
[65] Dreismann A, Ohadi H, del Valle-Inclan Redondo Y, et al. A sub-femtojoule electrical spin-switch based on optically trapped polariton condensates. Nat Mater 2016;15:1074–8.
[66] Khurgin JB. Excitonic radius in the cavity polariton in the regime of very strong coupling. Solid State Commun 2001;117:307.
[67] Christmann G, Simeonov D, Butté R, Feltin E, Carlin J-F, Grandjean N. Impact of disorder on high quality factor III-V nitride microcavities. Appl Phys Lett 2006;89:261101.
[68] Christopoulos S, von Högersthal GBH, Grundy AJD, et al. Room-temperature polariton lasing in semiconductor microcavities. Phys Rev Lett 2007;98:126405.
[69] Christmann G, Butté R, Feltin E, Carlin J-F, Grandjean N. Room temperature polariton lasing in a GaN/AlGaN multiple quantum well microcavity. Appl Phys Lett 2008;93:051102.
[70] Das A, Heo J, Jankowski M, et al. Room temperature ultralow threshold gan nanowire polariton laser. Phys Rev Lett 2011;107:066405.
[71] Li F, Orosz L, Kamoun O, et al. From excitonic to photonic polariton condensate in a zno-based microcavity. Phys Rev Lett 2013;110:196406.
[72] Bhattacharya P, Frost T, Deshpande S, Baten MZ, Hazari A, Das A. Room temperature electrically injected polariton laser. Phys Rev Lett 2014;112:236802.
[73] Michetti P, Mazza L, La Rocca G. in Organic nanophotonics. Nano-optics and nanophotonics (ed Zhao Y). Berlin: Springer, 2015, pp. 39–68.
[74] Agranovich VM, Litinskaia M, Lidzey DG. Cavity polaritons in microcavities containing disordered organic semiconductors. Phys Rev B 2003;67:085311.
[75] Scafirimuto F, Urbonas D, Scherf U, Mahrt RF, Stöferle T. Room-temperature exciton-polariton condensation in a tunable zero-dimensional microcavity. ACS Photonics 2018;5:85–9.

[76] Du M, Ribeiro RF, Yuen-Zhou J. Remote control of chemistry in optical cavities. 2018;arXiv:1810.10083 [quant-ph].
[77] Ballarini D, De Giorgi M, Gambino S, et al. polariton induced enhanced emission from an organic dye under strong coupling regime. Adv Opt Mater 2014;2:1076.
[78] Schwartz T, Hutchison JA, Genet C, Ebbesen TW. Reversible switching of ultrastrong light-molecule coupling. Phys Rev Lett 2011;106:196405.
[79] Kleemann M-E, Chikkaraddy R, Alexeev EM, et al. Strong-coupling of WSe2 in ultra-compact plasmonic nanocavities at room temperature. Nat Commun 2017;8:1296.
[80] D'Innocenzo V, Grancini G, Alcocer MJP, et al. Excitons versus free charges in organo-lead tri-halide perovskites. Nat Commun 2014;5:3586.
[81] Su R, Diederichs C, Wang J, et al. Room-temperature polariton lasing in all-inorganic perovskite nanoplatelets. Nano Lett 2017;17:3982–8.
[82] Fieramosca A, De Marco L, Passoni M, et al. Tunable out-of-plane excitons in 2D single crystal perovskites. ACS Photonics 2018;5:4179.
[83] Ballarini D, Amo A, Viña L, Sanvitto D, Skolnick MS, Roberts JS. Transition from the strong- to the weak-coupling regime in semiconductor microcavities: polarization dependence. Appl Phys Lett 2007;90:201905.
[84] Vladimirova M, Cronenberger S, Scalbert D, et al. Polarization controlled nonlinear transmission of light through semiconductor microcavities. Phys Rev B 2009;79:115325.
[85] Fieramosca A, Polimeno L, Ardizzone V, et al. Phys Opt 2018;arXiv:1811.04041.
[86] Gianfrate A, Dominici L, Voronych O, et al. Superluminal X-waves in a polariton quantum fluid. Light Sci Appl 2018;7:17119.
[87] Lerario G, Ballarini D, Fieramosca A, et al. High-speed flow of interacting organic polaritons. Light Sci Appl 2017;6:e16212.
[88] Todisco F, Esposito M, Panaro S, et al. Toward Cavity Quantum Electrodynamics with Hybrid Photon Gap-Plasmon States. ACS Nano 2016;10:11360–8.
[89] Deng H, Weihs G, Santori C, Bloch J, Yamamoto Y. Condensation of semiconductor microcavity exciton polaritons. Science 2002;298:199–202.
[90] Kasprzak J, Richard M, Kundermann S, et al. Bose-Einstein condensation of exciton polaritons. Nature 2006;443:449–14.
[91] Amo A, Sanvitto D, Laussy FP, et al. Collective fluid dynamics of a polariton condensate in a semiconductor microcavity. Nature 2009;457:291–5.
[92] Amo A, Lefrére J, Pigeon S, et al. Superfluidity of polaritons in semiconductor microcavities. Nat Phys 2009;5:805–10.
[93] Abbarchi M, Amo A, Sala VG, et al. Macroscopic quantum self-trapping and Josephson oscillations of exciton polaritons. Nat Phys 2013;9:275–9.
[94] Lagoudakis KG, Pietka B, Wouters M, André R, Deveaud-Plédran B. Coherent oscillations in an exciton-polariton Josephson junction. Phys Rev Lett 2010;105:120403.
[95] Sanvitto D, Pigeon S, Amo A, et al. All-optical control of the quantum flow of a polariton condensate. Nat Photonics 2011;5:610–4.
[96] Lagoudakis KG, Wouters M, Richard M, et al. Quantized vortices in an exciton-polariton condensate. Nat Phys 2008;4:706–10.
[97] Dominici L, Dagvadorj G, Fellows JM, et al. Vortex and half-vortex dynamics in a nonlinear spinor quantum fluid. Sci Adv 2015;1: e1500807.
[98] Kavokin A, Malpuech G, Glazov M. Optical spin Hall effect. Phys Rev Lett 2005;95:136601.
[99] Steger M, Liu G, Nelsen B, et al. Long-range ballistic motion and coherent flow of long-lifetime polaritons. Phys Rev B 2013;88:235314.
[100] Nelsen B, Liu G, Steger M, et al. Dissipationless flow and sharp threshold of a polariton condensate with long lifetime. Phys Rev X 2013;3:041015.
[101] Sun Y, Wen P, Yoon Y, et al. Bose-einstein condensation of long-lifetime polaritons in thermal equilibrium. Phys Rev Lett 2017;118:016602.
[102] Caputo D, Ballarini D, Dagvadorj G, et al. Topological order and thermal equilibrium in polariton condensates. Nat Mater 2018;17:145–51.
[103] Ballarini D, Caputo D, Sánchez Muñoz C, et al. Macroscopic two-dimensional polariton condensates. Phys Rev Lett 2017;118:215301.
[104] Karzig T, Bardyn C-E, Lindner NH, Refael G. Topological polaritons. Phys Rev X 2015;5:031001.
[105] Baboux F, Ge L, Jacqmin T, et al. Bosonic condensation and disorder-induced localization in a flat band. Phys Rev Lett 2016;116:066402.
[106] Klembt S, Harder TH, Egorov OA, et al. Exciton-polariton topological insulator. Nature 2018;562:552–6.
[107] Peter E, Senellart P, Martrou D, et al. Exciton-photon strong-coupling regime for a single quantum dot embedded in a microcavity. Phys Rev Lett 2005;95:067401.
[108] Reithmaier JP, Sek G, Löffler A, et al. Strong coupling in a single quantum dot–semiconductor microcavity system. Nature 2004;432:126405.
[109] Yoshie T, Scherer A, Hendrickson J, et al. Vacuum Rabi splitting with a single quantum dot in a photonic crystal nanocavity. Nature 2004;432:200–3.
[110] Hennessy K, Badolato A, Winger M, et al. Quantum nature of a strongly coupled single quantum dot–cavity system. Nature 2007;445:896–9.
[111] Press D, Götzinger S, Reitzenstein S, et al. Strong coupling of single quantum dots to micropillars. Phys Rev Lett 2007;98:117402.
[112] Schneider C, Gold P, Reitzenstein S, Höfling S, Kamp M. Quantum dot micropillar cavities with quality factors exceeding 250,000. Appl Phys B 2016;122:19.
[113] Boulier T, Bamba M, Amo A, et al. Polariton-generated intensity squeezing in semiconductor micropillars. Nat Commun 2014;5:3260.
[114] Adiyatullin AF, Anderson MD, Flayac H, et al. Periodic squeezing in a polariton Josephson junction. Nat Commun 2017;8:1329.
[115] Verger A, Ciuti C, Carusotto I. Polariton quantum blockade in a photonic dot. Phys Rev B 2006;73:193306.
[116] Snijders HJ, Frey JA, Norman J, et al. Observation of the unconventional photon blockade. Phys Rev Lett 2018;121:043601.
[117] Delteil A, Fink T, Schade A, Hofling S, Schneider C, Imamoglu A. Quantum correlations of confined exciton-polaritons. 2018;arXiv:1805.04020 [cond-mat.mes-hall].
[118] Muñoz-Matutano G, Wood A, Johnson M, et al. 2017;arXiv:1712.05551 [cond-mat.mes-hall].
[119] Cuevas Á, López Carreño JC, Silva B, et al. First observation of the quantized exciton-polariton field and effect of interactions on a single polariton. Sci Adv 2018;4:eaao6814.
[120] Lidzey DG, Bradley DDC, Virgili T, Armitage A, Skolnick MS, Walker S. Room temperature polariton emission from strongly

coupled organic semiconductor microcavities. Phys Rev Lett 1999;82:3316–9.
[121] Plumhof JD, Stöferle T, Mai L, Scherf U, Mahrt RF. Room-temperature Bose–Einstein condensation of cavity exciton–polaritons in a polymer. Nat Mater 2014;13:247–52.
[122] Lerario G, Fieramosca A, Barachati F, et al. Room-temperature superfluidity in a polariton condensate. Nat Phys 2017;13:837–41.
[123] Tinkler L, Walker P, Skryabin D, et al. Ultra-low-power hybrid light–matter solitons. Nat Commun 2014;6:9317.
[124] Lerario G, Cannavale A, Ballarini D, et al. Room temperature Bloch surface wave polaritons. Opt Lett 2014;39:2068.
[125] Pirotta S, Patrini M, Liscidini M, et al. Strong coupling between excitons in organic semiconductors and Bloch surface waves. Appl Phys Lett 2014;104:051111.
[126] Liscidini M, Gerace D, Sanvitto D, Bajoni D. Guided Bloch surface wave polaritons. Appl Phys Lett 2011;98:121118.
[127] Kaliteevski M, Iorsh I, Brand S, et al. Tamm plasmon-polaritons: Possible electromagnetic states at the interface of a metal and a dielectric Bragg mirror. Phys Rev B 2007;76:165415.
[128] Barachati F, Fieramosca A, Hafezian S, et al. Interacting polariton fluids in a monolayer of tungsten disulfide. Nat Nanotechnol 2018;13:906–9.
[129] Wurdack M, Lundt N, Klaas M, et al. Observation of hybrid Tamm-plasmon exciton- polaritons with GaAs quantum wells and a MoSe2 monolayer. Nat Commun 2017;8:259.
[130] Lundt N, Klembt S, Cherotchenko E, et al. Room-temperature Tamm-plasmon exciton-polaritons with a WSe2 monolayer. Nat Commun 2016;7:13328.
[131] Kristensen PT, Hughes S. Modes and mode volumes of leaky optical cavities and plasmonic nanoresonators. ACS Photonics 2014;1:2.
[132] Törmä P, Barnes W. Strong coupling between surface plasmon polaritons and emitters: a review. Rep Prog Phys 2015;78:013901.
[133] Bellessa J, Bonnand C, Plenet JC, Mugnier J. Strong coupling between surface plasmons and excitons in an organic semiconductor. Phys Rev Lett 2004;93:036404.
[134] Symonds C, Bonnand C, Plenet JC, et al. Particularities of surface plasmon–exciton strong coupling with large Rabi splitting. New J Phys 2008;10:065017.
[135] Hakala TK, Toppari JJ, Kuzyk A, et al. Vacuum rabi splitting and strong-coupling dynamics for surface-plasmon polaritons and rhodamine 6G molecules. Phys Rev Lett 2009;103:053602.
[136] Aberra Guebrou S, Symonds C, Homeyer E, et al. Coherent emission from a disordered organic semiconductor induced by strong coupling with surface plasmons. Phys Rev Lett 2012;108:066401.
[137] Todisco F, De Giorgi M, Esposito M, et al. Ultrastrong plasmon–exciton coupling by dynamic molecular aggregation. ACS Photonics 2018;5:143–50.
[138] Kato F, Minamimoto H, Nagasawa F, Yamamoto YS, Itoh T, Murakoshi K. Active tuning of strong coupling states between dye excitons and localized surface plasmons via electrochemical potential control. ACS Photonics 2018;5:788–96.
[139] Groß H, Hamm JM, Tufarelli T, Hess O, Hecht B. Near-field strong coupling of single quantum dots. Sci Adv 2018;4:eaar4906.
[140] Leng H, Szychowski B, Daniel M-C, Pelton M. Strong coupling and induced transparency at room temperature with single quantum dots and gap plasmons. Nat Commun 2018;9:4012.
[141] Faure S, Guillet T, Lefebvre P, Bretagnon T, Gil B. Comparison of strong coupling regimes in bulk GaAs, GaN, and ZnO semiconductor microcavities. Phys Rev B 2008;78:235323.
[142] Dufferwiel S, Schwarz S, Withers F, et al. Exciton–polaritons in van der Waals heterostructures embedded in tunable microcavities. Nat Commun 2015;6:8579.
[143] Liu W, Lee B, Naylor CH, et al. Strong Exciton–plasmon coupling in MoS2 coupled with plasmonic lattice. Nano Lett 2016;16:1262–9.
[144] Liu X, Galfsky T, Sun Z, et al. Strong light–matter coupling in two-dimensional atomic crystals. Nat Phys 2015;9:30–4.
[145] Cacciola A, Di Stefano O, Stassi R, Saija R, Savasta S. Ultrastrong coupling of plasmons and excitons in a nanoshell. ACS Nano 2014;8:11483. pMID: 25337782.
[146] Vasa P, Pomraenke R, Schwieger S, et al. Coherent exciton–surface-plasmon-polariton interaction in hybrid metal-semiconductor nanostructures. Phys Rev Lett 2008;101:116801.
[147] Väkeväinen AI, Moerland RJ, Rekola HT, et al. Plasmonic surface lattice resonances at the strong coupling regime. Nano Lett 2014;14:1721–7.
[148] De Giorgi M, Ramezani M, Todisco F, et al. Interaction and coherence of a plasmon–exciton polariton condensate. ACS Photonics 2018;5:3666–72.
[149] De Liberato S, Ciuti C. Quantum model of microcavity intersubband electroluminescent devices. Phys Rev B 2008;77:155321.
[150] De Liberato S, Ciuti C, Phillips CC. Terahertz lasing from intersubband polariton-polariton scattering in asymmetric quantum wells. Phys Rev B 2013;87:241304.
[151] Zanotto S, Mezzapesa FP, Bianco F, et al. Perfect energy-feeding into strongly coupled systems and interferometric control of polariton absorption. Nat Phys 2014;10:830–4.
[152] Alpeggiani F, Andreani LC. Quantum theory of surface plasmon polaritons: planar and spherical geometries. Plasmonics 2014;9:965.
[153] Colombelli R, Manceau J-M. Perspectives for intersubband polariton lasers. Phys Rev X 2015;5:011031.
[154] Askenazi B, Vasanelli A, Todorov Y, et al. Midinfrared ultrastrong Light–matter coupling for THz thermal emission. ACS Photonics 2017;4:2550.
[155] Manceau J-M, Tran N-L, Biasiol G, et al. Resonant intersubband polariton-LO phonon scattering in an optically pumped polaritonic device. Appl Phys Lett 2018;112:191106.
[156] Ciuti C, Bastard G, Carusotto I. Quantum vacuum properties of the intersubband cavity polariton field. Phys Rev B 2005;72:115303.
[157] Günter G, Anappara AA, Hees J, et al. Sub-cycle switch-on of ultrastrong light–matter interaction. Nature 2009;458:178.
[158] Dini D, Köhler R, Tredicucci A, Biasiol G, Sorba L. Microcavity polariton splitting of intersubband transitions. Phys Rev Lett 2003;90:116401.
[159] Anappara AA, De Liberato S, Tredicucci A, et al. Signatures of the ultrastrong light-matter coupling regime. Phys Rev B 2009;79:201303.
[160] Todorov Y, Andrews AM, Colombelli R, et al. Ultrastrong light-matter coupling regime with polariton dots. Phys Rev Lett 2010;105:196402.
[161] Malerba M, Ongarello T, Paulillo B, et al. Towards strong light-matter coupling at the single-resonator level with

sub-wavelength mid-infrared nano-antennas. Appl Phys Lett 2016;109:021111.
[162] Benz A, Campione S, Liu S, et al. Strong coupling in the sub-wavelength limit using metamaterial nanocavities. Nat Commun 2013;4:2882.
[163] Benz A, Campione S, Klem JF, Sinclair MB, Brener I. Control of strong light–matter coupling using the capacitance of metamaterial nanocavities. Nano Lett 2015;15:1959–66.
[164] Hagenmüller D, De Liberato S, Ciuti C. Ultrastrong coupling between a cavity resonator and the cyclotron transition of a two-dimensional electron gas in the case of an integer filling factor. Phys Rev B 2010;81:235303.
[165] Muravev VM, Andreev IV, Kukushkin IV, Schmult S, Dietsche W. Observation of hybrid plasmon-photon modes in microwave transmission of coplanar microresonators. Phys Rev B 2011;83:075309.
[166] Scalari G, Maissen C, Turcinkova D, et al. Ultrastrong coupling of the cyclotron transition of a 2D electron Gas to a THz metamaterial. Sci 2012;335:1323.
[167] Scalari G, Maissen C, Hagenmüller D, et al. Ultrastrong light-matter coupling at terahertz frequencies with split ring resonators and inter-Landau level transitions. J Appl Phys 2013;113:136510.
[168] Bayer A, Pozimski M, Schambeck S, et al. Terahertz light–matter interaction beyond unity coupling strength. Nano Lett 2017;17:6340–4.
[169] Zhang Q, Lou M, Li X, et al. Collective non-perturbative coupling of 2D electrons with high-quality-factor terahertz cavity photons. Nat Phys 2016;12:1005–11.
[170] Li X, Bamba M, Zhang Q, et al. Vacuum Bloch–Siegert shift in landau polaritons with ultra-high cooperativity. Nat Photonics 2018;12:324.
[171] Keller J, Scalari G, Cibella S, et al. Few-Electron ultrastrong light-matter coupling at 300 GHz with nanogap hybrid LC microcavities. Nano Lett 2017;17:7410–5.
[172] Hillenbrand R, Taubner T, Keilmann F. Phonon-enhanced light–matter interaction at the nanometre scale. Nature 2002;418:159–62.
[173] Wang T, Li P, Hauer B, Chigrin DN, Taubner T. Optical properties of single infrared resonant circular microcavities for surface phonon polaritons. Nano Lett 2013;13:5051–5.
[174] Caldwell JD, Glembocki OJ, Francescato Y, et al. Low-loss, extreme sub-diffraction photon confinement via silicon carbide surface phonon polariton nanopillar resonators. Nano Lett 2013;13:3690–7.
[175] Caldwell JD, Lindsay L, Giannini V et al. Low-loss, infrared and terahertz nanophotonics using surface phonon polaritons. Nanophotonics 2015;4:44.
[176] Gubbin CR, Maier SA, De Liberato S. Theoretical investigation of phonon polaritons in SiC micropillar resonators. Phys Rev B 2017;95:035313.
[177] Wang T, Li P, Chigrin DN, et al. Phonon-Polaritonic bowtie nanoantennas: Controlling infrared thermal radiation at the nanoscale. ACS Photonics 2017;4:1753–60.
[178] Gubbin CR, De Liberato S. Theory of Four-Wave-Mixing in phonon polaritons. ACS Photonics 2018;5:284.
[179] Razdolski I, Passler NC, Gubbin CR, et al. Second harmonic generation from strongly coupled localized and propagating phonon-polariton modes. Phys Rev B 2018;98:125425.
[180] Huck C, Vogt J, Neuman T, et al. Strong coupling between phonon-polaritons and plasmonic nanorods. Opt Express 2016;24:25528.
[181] Li K, Fitzgerald JM, Xiao X, et al. Graphene plasmon cavities made with silicon carbide. ACS Omega 2017;2:3640–6.
[182] Gubbin CR, Martini F, Politi A, Maier SA, De Liberato S. Strong and coherent coupling between localized and propagating phonon polaritons. Phys Rev Lett 2016;116:246402.
[183] Passler NC, Gubbin CR, Folland TG, et al. Strong coupling of Epsilon-Near-Zero phonon polaritons in polar dielectric heterostructures. Nano Lett 2018;18:4285–92.
[184] Othani K, Meng B, Franckié M, et al. Raman emission from an electrically pumped phonon polariton laser. 2018;arXiv:1808.09844.
[185] Franckié M, Ndebeka-Bandou C, Ohtani K, Faist J. Quantum model of gain in phonon-polariton lasers. Phys Rev B 2018;97:075402.